Electronic Supplementary Material (ESI) for Nanoscale.

Supporting Information

Title: Structure evolution and energy storage mechanism of $Zn_3V_3O_8$ spinel in aqueous zinc batteries

Haocong Yi[1], Changjian Zuo[1], Hengyu Ren, Wenguang Zhao, Yuetao Wang, Shouxiang Ding, Yang Li, Runzhi Qin*, Lin Zhou, Lu Yao, Shunning Li, Qinghe Zhao*, Feng Pan*

(School of Advanced Materials, Peking University Shenzhen Graduate School, Shenzhen 518055, PR China)

Responding authors: bushihaoren@pku.edu.cn; zhaoqh@pku.edu.cn; panfeng@pkusz.edu.cn

Table S1 ICP results of Zn and V in s-ZnVO powder

Elements	Zn	V	Zn/V ratio
Concentration	23.98 μg mL^{-1}	16.98 μg mL^{-1}	1.1

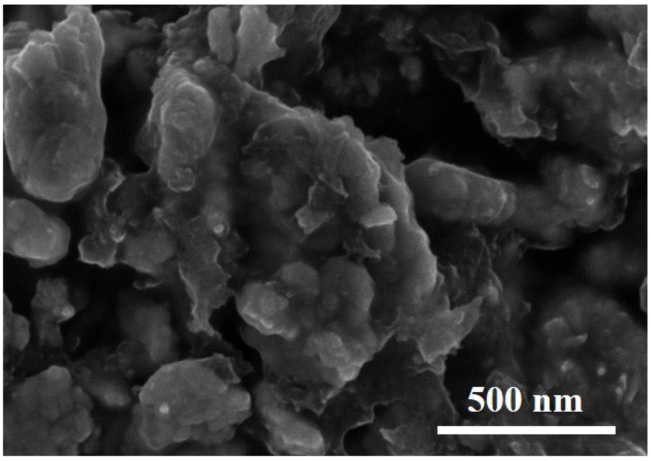

Figure S1 SEM morphology of $Zn_3V_3O_8$ spinel powder.

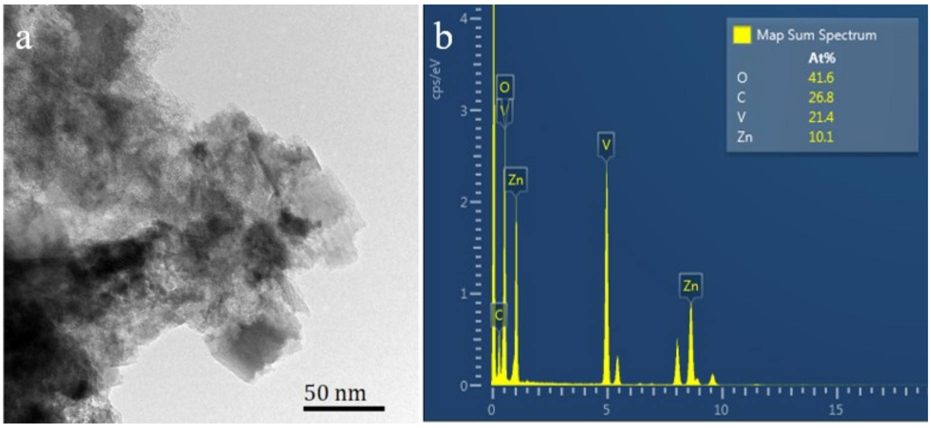

Figure S2 (a) TEM morphology and (b) EDS elemental result of $Zn_3V_3O_8$ spinel powder.

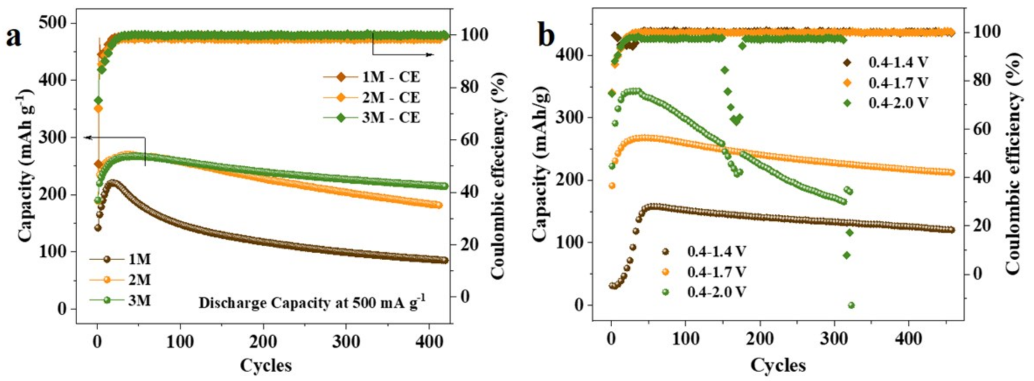

Figure S3 Tuning cell performance of $Zn/Zn_3V_3O_8$ cells. (a) Comparison of cell performances in electrolytes with 1 M, 2 M, and 3 M $Zn(CF_3SO_3)_2$, cell voltage ranges of 0.4-1.7 V. (b) Comparison of cell performances in electrolytes with cell voltage ranges of 0.4-1.4 V, 0.4-1.7 V, and 0.4-2.0 V, and in 3 M $Zn(CF_3SO_3)_2$ electrolyte.

In this work, the electrolyte concentration and cutoff voltage (COV) are comprehensively tuned to explore the optimized electrode performances, as shown in **Figure S3**. The result in **Figure S3a** shows that increasing electrolyte concentration from 1M to 3M, the capacity delivery became higher with enhanced cycling stability, mainly due to the variated proton and Zn^{2+} ion insertion processes in the cathode/electrolyte interface. Meanwhile, the result in **Figure S3b** indicates that elevating the COV help to achieve more capacity release, but greatly reduce the cycle stability, mainly attributing to the more severe vanadium dissolution, and more serious structure variation upon cycle induced by higher COV. Specially, under the voltage range of 0.4-2.0 V, some fluctuation in the middle of the curve, illustrating the precarious situation of ZnVO electrode. Thus, 3M $Zn(CF_3SO_3)_2$ electrolyte and a COV value of ~1.7 V vs. Zn/Zn^{2+} can be the optimized electrochemical condition for $Zn/Zn_3V_3O_8$ cells.

Table S2 Electrode performances of reported spinel-type host materials in aqueous Zn-ion batteries.

Compounds	Capacity	Rate performance	Cycling stability	Reference
$Zn_3V_3O_8$	**294 mAh g^{-1} at 0.1 A g^{-1}.**	**229 mAh g^{-1} at 2.0 A g^{-1}**	**CR of 74.6%, in 1200 cycles, at 2.0 A g^{-1}**	**This work**
Cation-deficient $ZnMn_2O_4$	150 mAh g^{-1} at 0.05 A g^{-1}.	75 mAh g^{-1} at 2.0 A g^{-1}.	CR of 94%, in 500 cycles, at 0.5 A g^{-1}	J. Am. Chem. Soc. 2016, 138, 12894.
$ZnMn_2O_4$@C	194 mAh g^{-1} at 0.1 A g^{-1}	132 mAh g^{-1} at 3.0 A g^{-1}.	CR of 84%, in 2000 cycles, at 3.0 A g^{-1}	Adv. Sci. 2020, 2002636.
ZnV_2O_4	312 mAh g^{-1} at 0.5C	174 mAh g^{-1} at 20C.	CR of 74%, in 1000 cycles, at 10C	Nano Energy, 2019, 104211.
$ZnMnCoO_4$	109.4 mAh g^{-1} at 0.05 A g^{-1}	54 mAh g^{-1} at 0.2 A g^{-1}	CR of 74%, in 120 cycles, at 10C	ACS Appl. Energy Mater. 2019, 2, 3211−3219
$ZnAl_xCo_{2-x}O_4$	134 mAh g^{-1} at 0.2C	14.16 mAh g^{-1} at 10C.	CR of 85%, in 100 cycles, at 0.2C	Chem. Mater. 2017, 29, 9351-9359
$Zn_{1.67}Mn_{1.33}O_4$	330 mAh g^{-1} at 0.5C	50 mAh g^{-1} at 1C.	CR of 53%, in 40 cycles, at 0.1C	Journal of Alloys and Compounds 800 (2019) 478e482
$ZnNi_{1/2}Mn_{1/2}CoO_4$	180 mAh g^{-1} at 0.2C	108 mAh g^{-1} at 5C.	CR of 90%, in 200 cycles, at 0.2C	Adv. Energy Mater. 2018, 8, 1800589
$ZnMn_2O_4$@PCPs	176.8 mAh g^{-1} at 0.1 A g^{-1}	88.7 mAh g^{-1} at 4 A g^{-1}	CR of 90.3%, in 2000 cycles, at 1 A g^{-1}	Journal of Power Sources 452 (2020) 227826
MgV_2O_4	272 mAh g^{-1} at 0.2 A g^{-1}	170 mAh g^{-1} at 5.0 A g^{-1}.	CR of 64%, in 500 cycles, at 4.0 A g^{-1}	ACS Sustainable Chem. Eng. 2020, 8, 3681−3688

Notes: CR represents “capacity retention”.

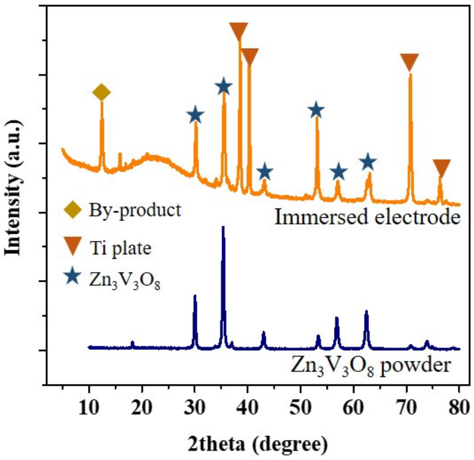

Figure S4 XRD patterns of $Zn_3V_3O_8$ electrode immersing in 3 M $Zn(CF_3SO_3)_2$ electrolyte for 12 h

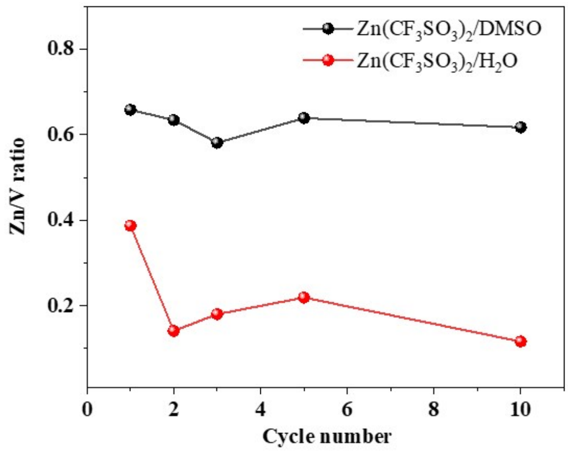

Figure S5 Zn/V ratio variation curves of $Zn_3V_3O_8$ electrode during cycling in rate current of 200 mA g^{-1}.

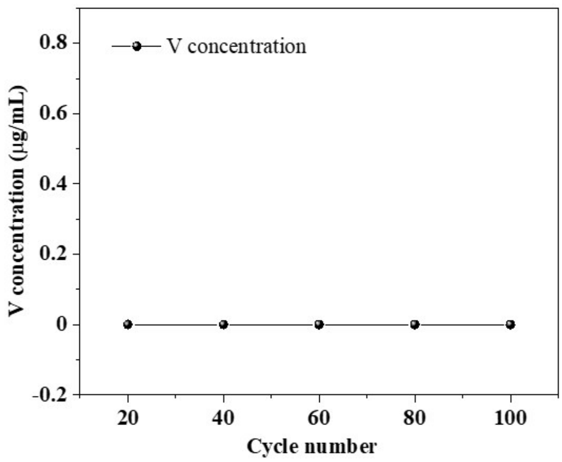

Figure S6 V concentrations in electrolytes during cycling of $Zn_3V_3O_8$ electrodes at 500 mA g^{-1}, based on the ICP-OES results.

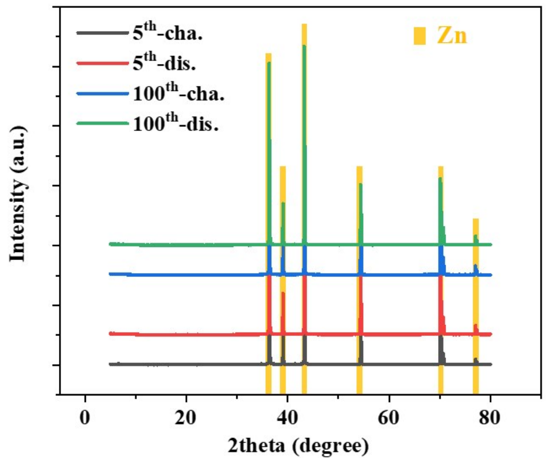

Figure S7 XRD patterns of Zn anodes during cycling at current of 500 mA g^{-1}

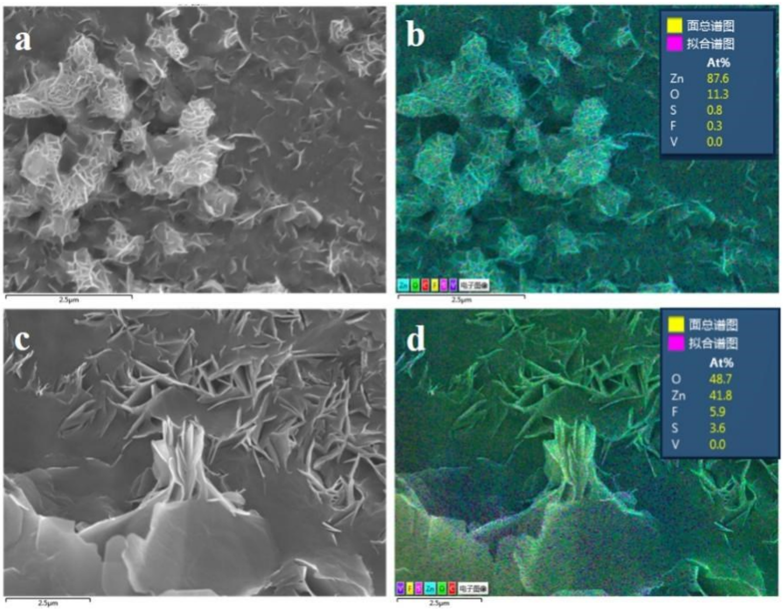

Figure S8 SEM morphologies of Zn anodes at (a, b)5th and (c, d) 100th cycles at current of ~500 mA g^{-1}.

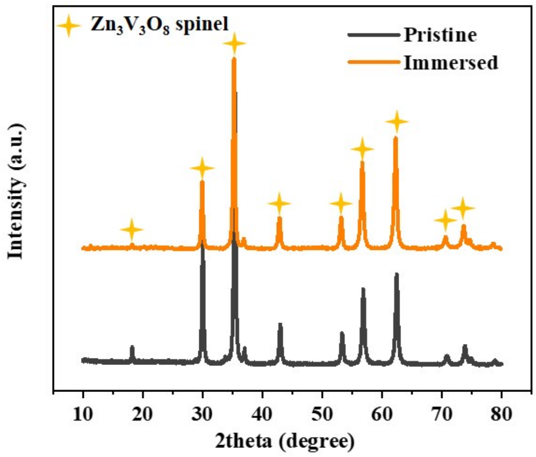

Figure S9 Comparison of XRD patterns of pristine and immersed $Zn_3V_3O_8$ products in diluted H_2SO_4 electrolyte.

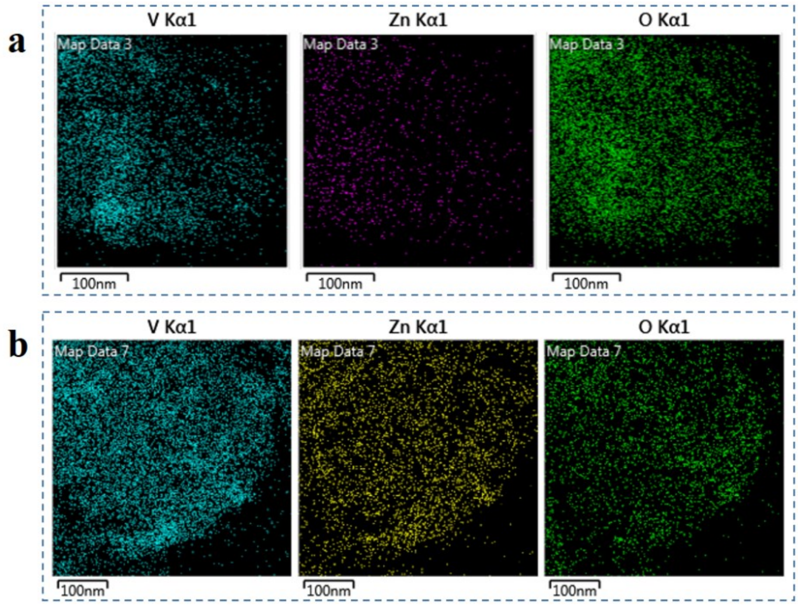

Figure S10 TEM-EDS mapping results of $Zn_3V_3O_8$ electrode at (a) charged and (b) discharged states.

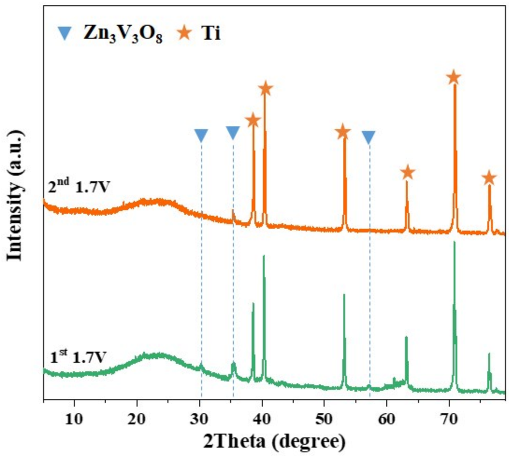

Figure S11 XRD patterns of $Zn_3V_3O_8$ electrode at charged and discharged states in 1st and 2nd cycle in DMSO electrolyte

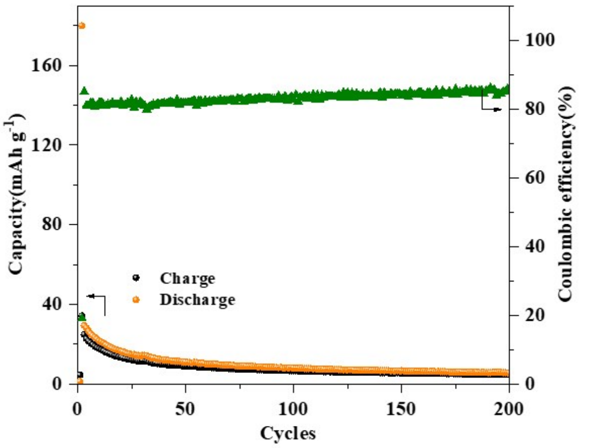

Figure S12 Electrochemical performances of $Zn_3V_3O_8$ electrode in 0.3M $Zn(CF_3SO_3)_2$/DMSO electrolyte.

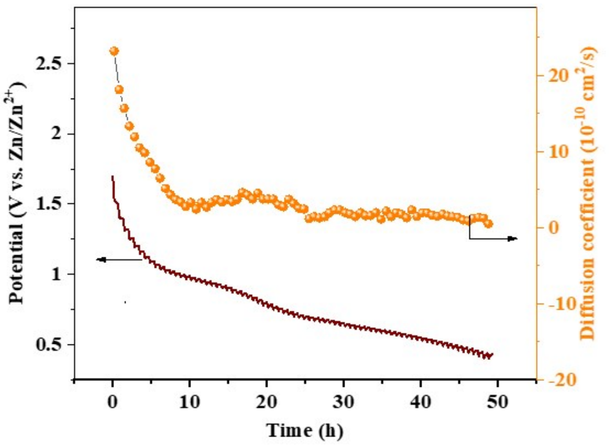

Figure S13 GITT calculations of diffusion kinetics of $Zn_3V_3O_8$ electrode in 3M $Zn(CF_3SO_3)_2$ electrolyte

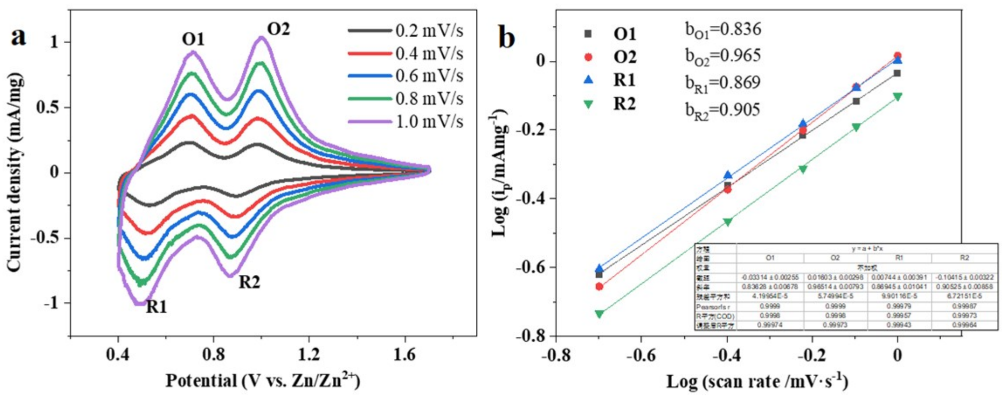

Figure S14 (a) CV curves of $Zn_3V_3O_8$ electrode in 3M $Zn(CF_3SO_3)_2$ electrolyte at different scanning rates; (b) corresponding linear-fitting of log(current)-log(scan rate) curves

Table S3 Diffusion coefficients reported in literatures

Samples	Diffusion kinetics ($cm^2 s^{-1}$)	References
ZnV_2O_4	$7*10^{-10}$	Nano Energy 67 (2019) 104211
MgV_2O_4	10^{-11} to 10^{-10}	ACS Sustainable Chem. Eng. 8 (2020) 3681-3688.
Oxygen-deficient V_6O_{13}	$1.1*10^{-11}$	Angew. Chem. Int. Ed. 59 (2020) 2273-2278.
V_2O_5-PANI	$1.02*10^{-10}$	Adv. Mater. (2020) 2001113.
VO_2-PEDOT	10^{-8} to 10^{-9}	J. Power Sources 463 (2020) 228223.
PANI-$V_2O_5·nH_2O$	$5.6*10^{-16}$ at 1.6 V to $3.6*10^{-13}$ at 0.4 V	ACS Appl. Mater. Interfaces, 12 (2020) 31564-31574.
$Na_2V_6O_{16}·1.63H_2O$	$1.24*10^{-13}$	Nano Lett. 18 (2018) 1758-1763.
$Ni_{0.25}V_2O_5·0.88H_2O$	$3.4*10^{-12}$	ACS Appl. Mater. Interfaces 12 (2020) 24726-24736.
$Li_xV_2O_5·nH_2O$	$0.95*10^{-8}$ to $3.37*10^{-8}$	Energy Environ. Sci. 11 (2018) 3157-3162.
MnVO	$3.22*10^{-12}$	Energy Environ. Sci. 12 (2019) 2273-2285.
VO_2	$10^{-5.6}$ to $10^{-7.5}$	Chem. Mater. 31 (2019) 699-706.
$K_{0.23}V_2O_5$	$1.88*10^{-9}$ to $2.6*10^{-8}$	J. Alloys Compd. 819 (2020) 152971
$(NH_4)_2V_6O_{16}·1.5H_2O$	$1.04*10^{-12}$ to $2.63*10^{-11}$	J. Power Sources 441 (2019) 227192
V_6O_{13}	$5*10^{-9}$ to $2.4*10^{-8}$	Energy Technol. 7 (2019) 1900022
$(Na,Mn)V_8O_{20}·nH_2O$	$1.9*10^{-9}$ to $2.5*10^{-10}$	Adv. Sci. 7 (2020) 2000083
PANI/V_2O_5 composite	10^{-9} to 10^{-10}	Chemical Engineering Journal 399 (2020) 125842
$(NH_4)_2V_7O_{16}·3.2H_2O$	10^{-10} to 10^{-12}	ACS Appl. Mater. Interfaces 13 (2021) 5034-5043
$NH_4V_4O_{10}$	10^{-10} to 10^{-12}	Nano-Micro Lett. 13 (2021) 116